JMEPEG (2017) 26:2118–2128
DOI: 10.1007/s11665-017-2662-2

1059-9495/$19.00

Effect of Surface Roughness and Structure Features on Tribological Properties of Electrodeposited Nanocrystalline Ni and Ni/Al_2O_3 Coatings

Anna Góral, Lidia Lityńska-Dobrzyńska, and Marcin Kot

(Submitted January 30, 2017; in revised form March 28, 2017; published online April 13, 2017)

Metal matrix composite coatings obtained by electrodeposition are one of the ways of improving the surfaces of materials to enhance their durability and properties required in different applications. This paper presents an analysis of the surface topography, microstructure and properties (residual stresses, microhardness, wear resistance) of Ni/Al_2O_3 nanocomposite coatings electrodeposited on steel substrates from modified Watt's-type baths containing various concentrations of Al_2O_3 nanoparticles and a saccharin additive. The residual stresses measured in the Ni/Al_2O_3 coatings decreased with an increasing amount of the co-deposited ceramics. It was established that the addition of Al_2O_3 powder significantly improved the coatings' microhardness. The wear mechanism changed from adhesive-abrasive to abrasive with a rising amount of Al_2O_3 particles and coating microhardness. Nanocomposite coatings also exhibited a lower coefficient of friction than that of a pure Ni-electrodeposited coating. The friction was found to depend on the surface roughness, and the smoother surfaces gave lower friction coefficients.

Keywords friction coefficient, metal matrix composite, Ni/nano-Al_2O_3, residual stresses, surface topography, wear

1. Introduction

Metal matrix composite (MMC) coatings reveal improved properties (compared to pure metal), derived from the co-deposition of dispersed hard particles in the metallic matrix. They are produced by different technologies, depending on the application and economic reasons. Several metals, e.g., nickel, copper or chromium, are mainly used as the metal matrix, whereas metal oxides, carbides, borides and polymers are the co-depositing particles (Ref 1-4). Electrochemical deposition is a method of covering conductive surfaces with metals or alloys as well as composite coatings aimed at obtaining the required surface characteristics. It enables control of the deposit microstructure and thickness as well manufacture of nanocrystalline coatings in a single step without secondary treatment (Ref 5). During the electrodeposition process of composite coatings, dispersed hard particles are kept in suspension in an electrolyte and then incorporated into the metal matrix. Through the application of different plating baths and different types of particles (oxides, carbides, graphite, sulfides and PTFE), the production of a large range of composite coatings exhibiting excellent properties, such as wear resistance, corrosion resistance and lubrication, depending on the type, amount and distribution of the co-deposited particles was possible (Ref 7-14). Moreover, increasingly popular are functionally graded nanocomposite coatings (e.g., Ni/Ni-Al_2O_3, Ni-W-Al_2O_3) into which alumina content increases from the substrate toward the surface of the coating possessing improved wear and corrosion resistance properties (Ref 15, 16). The incorporation of hard ceramic particles into the metallic matrix enables the manufacturing of composite coatings with enhanced mechanical and tribological properties as compared to pure metal coatings (Ref 9-12, 17, 18). Therefore, they are applied as the coatings reducing friction and wear in friction nodes (Ref 19, 20).

Ni/Al_2O_3 coatings are considered as potential candidates to replace electrodeposited hard chromium coatings, the production of which is limited by restrictive environmental laws (Ref 21-23). Ni/Al_2O_3 nanocomposite coatings are used primarily to increase the wear resistance of metal surfaces in microdevices. Due to their good tribological and anticorrosion properties, they find application as coatings of engine cylinders, high-pressure valves, and dies and in the production of car accessories and small aircraft and electrotechnical parts (Ref 24-26). Electrolytic nickel coatings exhibit specific properties, such as good corrosion resistance and catalytic activity in many electrochemical processes (Ref 27). Incorporating ceramic nanoparticles into the nickel matrix allows one to obtain higher microhardness and good wear properties (Ref 11, 28). Ni/Al_2O_3 have been extensively studied; however, considerable research has been focused on the impact of the electrodeposition parameters, especially the value and kind (direct, pulse) of the current density (Ref 11, 13, 29-31) as well as the type and concentration of the applied additives (Ref 5, 6), on the manufacture process and the volume fraction of the particles built in the nickel matrix. It is known that an addition of saccharin to the electrolytic bath causes grain size refinement of the materials (Ref 32-38). The microstructure refinement, in turn, has a significant impact on the mechanical wear properties of the coatings. Additionally, decreasing the ceramic particle size can also affect the properties in a positive way, mainly through the hardening of the metal matrix coatings by finely

Anna Góral and **Lidia Lityńska-Dobrzyńska**, Institute of Metallurgy and Materials Science of the Polish Academy of Sciences, 25 Reymonta St., 30-059 Kraków, Poland; and **Marcin Kot**, Faculty of Mechanical Engineering and Robotics, AGH University of Science and Technology, av. Mickiewicza 30, 30-059 Kraków, Poland. Contact e-mail: a.goral@imim.pl.

dispersed particles (Ref 31). To enhance the tribological properties of electrodeposited nanocomposite coatings, the interface between the nanoparticles and the metal matrix must have enough strength to ensure that the embedded particles are not torn out during tribological contact. Aruna et al. (Ref 12) have shown that the wear resistance of Ni/Al_2O_3 containing alpha alumina is higher than that of the composites containing gamma alumina and mixtures of alpha, gamma and delta alumina. Gul et al. (Ref 11) have compared the tribological properties of Ni/Al_2O_3 coatings produced by the way of applying both the direct (DC) and pulse (PC) current densities. They showed that the coating obtained with PC did not reveal a significant increase in hardness; it had a larger grain size and more plastic deformation compared with the DC-coated materials. Improving the abrasive resistance of the components is becoming a research subject of top priority and a great industrial importance. It is known that the friction coefficient and the wear resistance of a material are related to its surface topography and, usually, smoother surfaces give a lower friction coefficient (Ref 39-41). However, this relationship depends on the environmental conditions and on the material types of the two friction surfaces, as well as on the type of motion.

This paper presents the effect of the surface roughness of the thin nanocrystalline Ni and Ni/Al_2O_3 coatings electrodeposited from the Watt's bath containing various amounts of Al_2O_3 nanoparticles on their friction and wear resistance, which has not been investigated, yet. A novelty of this paper is also the linking the mechanical and tribological properties of the Ni/Al_2O_3 nanocomposite coatings with the structure features observed in nanoscale, especially growth-type nanotwins existing in the nickel matrix. Furthermore, the influence of a saccharin additive in the electrolytic bath on the microstructural features of Ni/Al_2O_3 coatings, depth-sensing indentation response, residual stresses and wear behavior has been investigated and compared with that of pure Ni and Ni/Al_2O_3 coatings obtained from the bath without an additive. The selection of saccharin was dictated by earlier examinations, which revealed higher microhardness and good anticorrosive properties of the resulting coatings (Ref 42).

2. Experimental Details

Nickel/alumina nanocomposite coatings were deposited electrochemically from a modified Watts bath containing 120 g/L $NiSO_4 \cdot 6H_2O$, 70 g/L $NiCl_2 \cdot 6H_2O$ and 50 g/L H_3BO_3 into which various amounts (20, 40, 60, 80 g/L) of α-Al_2O_3 nanopowder were added. These samples were denoted as: Ni, Ni/Al_2O_3-20, Ni/Al_2O_3-40, Ni/Al_2O_3-60 and Ni/Al_2O_3-80. Additionally, nanocomposite coatings produced from the bath, which, beside the 80 g/L of α-Al_2O_3, contained 1 g/L of saccharin, were also examined and denoted as Ni/Al_2O_3-80 + S. The size of the alumina particles ranged from 80 to 150 nm. The details regarding the electrodeposition of nickel/alumina coatings on low carbon steel substrates have already been published (Ref 13, 43). In order to identify the effect of the ceramic particles on the Ni/Al_2O_3 deposit properties, all the coatings were deposited using a potentiostat/galvanostat AUTOLAB model PGSTAT 302 under the same conditions: current density of 5 A/dm^2, pH 4, temperature of 40 °C, anode—a vertically placed nickel (99.9% purity) plate, and cathode—a vertically mounted low carbon steel disk with a diameter of 20 mm. Before the co-deposition, the alumina particles were ultrasonically dispersed in the bath for 2 h and mechanically agitated (800 rpm) using a magnetic stirrer. During the electrodeposition, the bath was stirred using a magnetic stirrer with a stirring rate of 500 rpm and circulated with a peristaltic pump (50 rpm). The obtained coatings were ultrasonically cleaned to remove particles loosely adherent to their surface. The thickness of the analyzed coatings was in the range of 9.7-12 μm. The coatings were completely characterized with the use of XRD techniques (Bruker D8 diffractometer with Co Kα filtered radiation) as well as scanning and transmission electron microscopes (SEM—FEI QUANTA 3D FEG, and TEM—FEI TECNAI G^2). The thin foils were prepared by the focused ion beam (FIB) technique with the use of an FEI Quanta 3D dual beam. The amount of Al_2O_3 nanoparticles incorporated into the Ni matrix was determined with the use of Loco's Shire dedicated to image analysis. The particles percentage by volume (vol.%) was determined based on ten areas of the SEM coating microstructures (8.9 μm × 14.7 μm) of the cross sections of the coatings. The residual stresses were measured based on the 311 Ni reflection (2θ = 114.9°)—with the use of the $\sin^2\psi$ method. The indentation technique (Ref 44, 45) was used to evaluate the hardness and the elasticity modulus. The tests were performed at the 50 mN maximum load and the 100 mN/min loading and unloading rate with the use of the CSEM-MCT equipment. On each coating, at least nine indentations were made, and for further analysis, the average values were taken. The tests of the wear and friction coefficient of Ni/Al_2O_3 coatings were performed under dry conditions with the use of a ball-on-disk tribometer [according to the ISO standard (Ref 46)] with 6-mm-diameter sintered α-Al_2O_3 spheres. The tests were performed at the temperature of 22 ± 2 °C with the relative humidity of 50 ± 2%. The normal load was 10 N, the linear sliding speed of the ball was 0.05 m/s, the radius was 7 mm, and the number of cycles was 20,000. Only for the Ni/Al_2O_3-80 + S wear, the index wear was calculated after 80,000 cycles. After the tests, the wear track profiles were measured, and then, the specific wear index W_V was calculated from the formula:

$$W_V = \frac{V}{F_n \cdot s}$$

where V—volume of the removed material calculated on the basis of the average cross-sectional area of the grooves, F_n—normal load, s—sliding distance. The worn surfaces were subjected to SEM observations for the analysis of the wear mechanism. The topography of the coatings after polishing was analyzed by means of a Talysurf CCI Lite non-contact 3D profiler (Ref 47).

3. Results and Discussion

3.1 Microstructure of Ni and Ni/Al_2O_3 Coatings

The SEM BSE surface morphologies of pure Ni and Ni/Al_2O_3-20, Ni/Al_2O_3-40, Ni/Al_2O_3-60, Ni/Al_2O_3-80, Ni/Al_2O_3-80 + S composite coatings are presented in Fig. 1. The pure Ni deposits exhibited a pyramidal microstructure on the surface, as shown in Fig. 1(a). The microstructure of the composite Ni/Al_2O_3 coatings was finer, with visible Al_2O_3 particles (fine dark areas), as shown in Fig. 1(b), (c), (d), (e), and (f). The composite coatings produced a flatter surface when compared to the nickel deposits. The coatings did not reveal any pores or

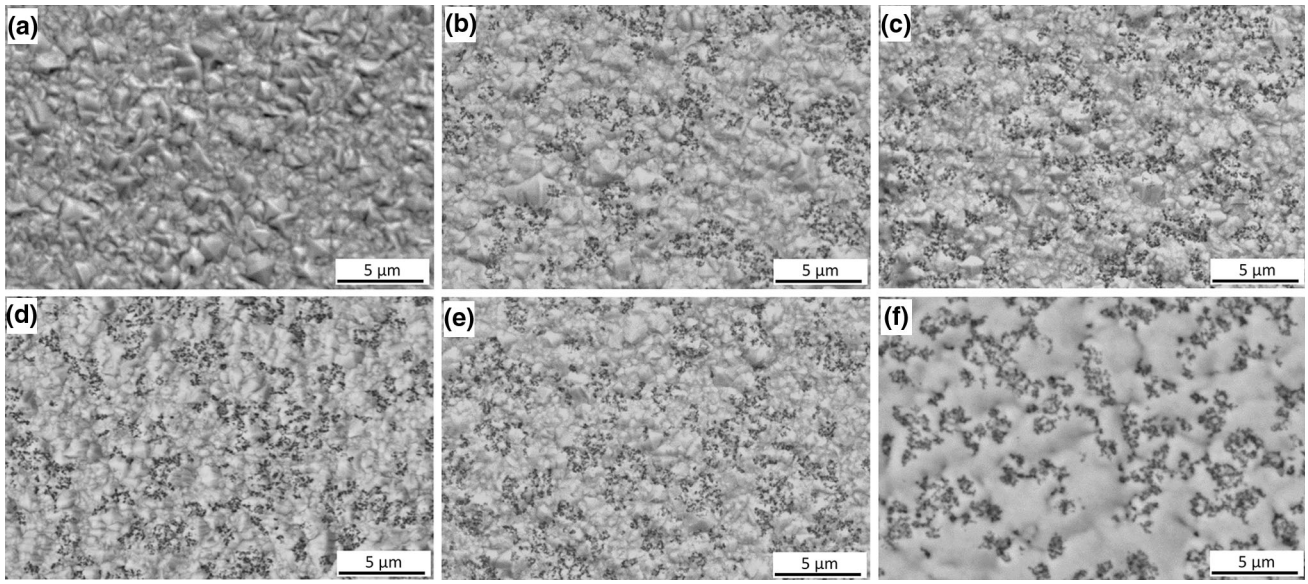

Fig. 1 SEM BSE microstructures of the surfaces of coatings: Ni (a), Ni/Al_2O_3-20 (b), Ni/Al_2O_3-40 (c), Ni/Al_2O_3-60 (d), Ni/Al_2O_3-80 (e), Ni/Al_2O_3-80 + S (f)

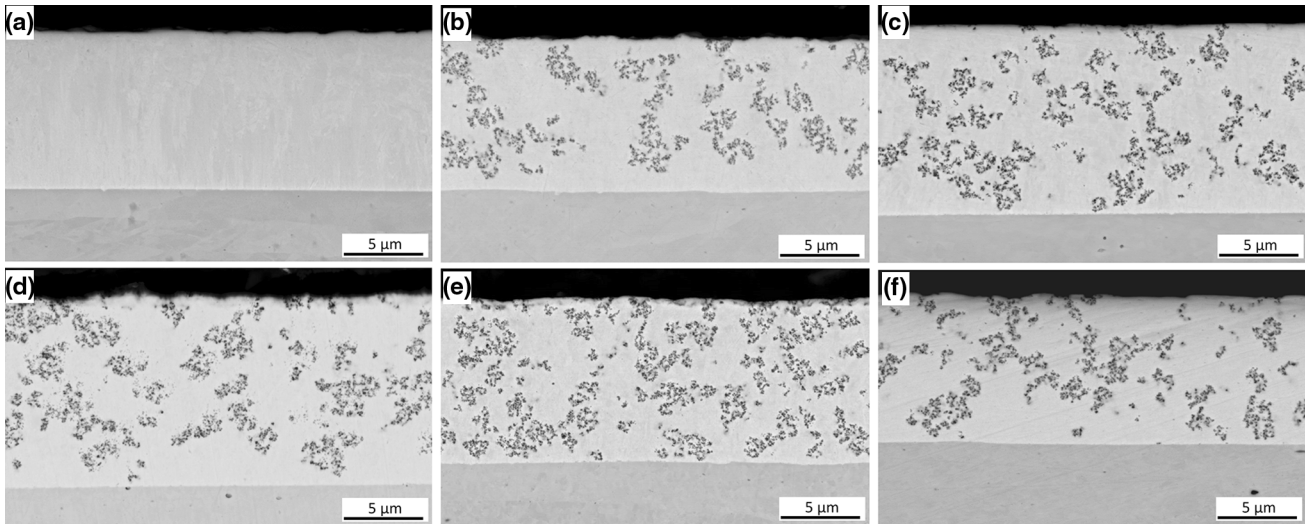

Fig. 2 SEM BSE microstructures of the cross sections of coatings: Ni (a), Ni/Al_2O_3-20 (b), Ni/Al_2O_3-40 (c), Ni/Al_2O_3-60 (d), Ni/Al_2O_3-80 (e), Ni/Al_2O_3-80 + S (f)

fissures on the surfaces. As can be seen from the cross sections presented in Fig. 2, all the produced coatings were compact. The nanoparticles present in the Ni matrix were usually concentrated in agglomerates, as shown in Fig. 2(b), (c), (d), (e), and (f). The distribution of agglomerates in the coating became more uniform with an increasing amount of Al_2O_3 nanoparticles added to the electrolyte. Furthermore, it is worth emphasizing that although these coatings were thin (9.7-12 µm), they revealed a uniform particle agglomerate distribution from the substrate to the coating surface. The Al_2O_3 nanoparticles had an influence on the crystallization behavior of the composite coatings. The surfaces of the Al_2O_3 nanoparticles provided new sites for the nucleation of nickel grains, so the amount of nucleation sites for the Ni grains was higher than for pure Ni. It was found that the Ni matrix grew in the form of columnar grains in all the coatings, which decreased in size with the alumina and saccharin additive (Fig. 3a, b, and c) and led to a fine-grained microstructure as shown in Fig. 3(c). The Ni and Ni/Al_2O_3 coatings revealed the presence of numerous nanotwins in the Ni matrix, which influence the mechanical properties of the coatings. The smallest matrix grains containing nanotwins were observed in the Ni/Al_2O_3-80 + S composite coating produced from the bath including saccharin. A detailed description of the Ni and Ni/Al_2O_3 coating microstructures containing nanotwins formed during electrodeposition was recorded in Ref 43. An increasing (from 20 to 80 g/L) amount of the ceramic phase in the electrolyte caused a rise of the amount of the ceramic particles from 7.9 to 9.9 vol.% embedded in the Ni matrix (Fig. 4), as was estimated on the basis of the SEM microstructures. These percentages by volume of the incorporated Al_2O_3 nanoparticles were comparable to those determined in Ref 11.

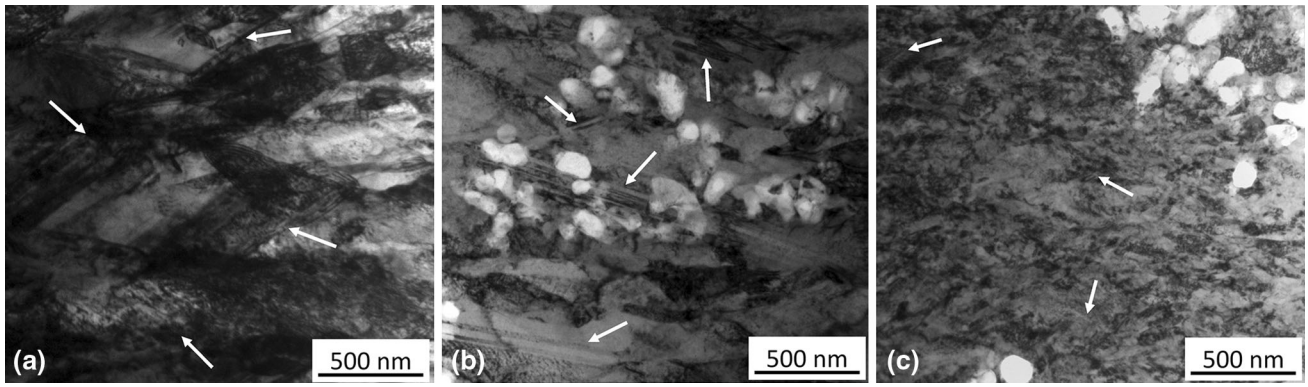

Fig. 3 Bright-field TEM image of the cross sections of coatings: Ni (a), Ni/Al_2O_3-80 (b), Ni/Al_2O_3-80 + S (c) with nanotwins marked with arrows

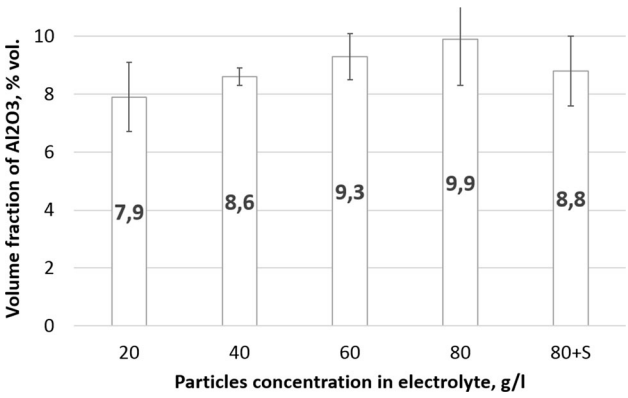

Fig. 4 Volume fraction of Al_2O_3 nanoparticles incorporated into coatings at various Al_2O_3 concentrations in the electrolyte

3.2 Surface Topography of Coatings

Four coating surface structures (Ni, Ni/Al_2O_3-20, Ni/Al_2O_3-80 Ni/Al_2O_3-80 + S) as regards their tribological behavior were characterized. The surface topography, depth histogram and bearing curve for the Ni and Ni/Al_2O_3 coatings are presented in Fig. 5. According to ISO 25178, the height parameters were calculated based on all the measurement data from the optically scanned surface area and are presented in Table 1. The parameters were derived from the Abbott-Firestone curve, which characterizes the functional behavior of the measured surface. As shown in Table 1, the arithmetic mean height S_a, giving a very good overall description of the height variations, was the highest (0.4147 μm) for the pure Ni coating and the lowest (0.228 μm) for Ni/Al_2O_3-80 + S. As shown in Table 1, the differences in the values of S_a for the examined Ni/Al_2O_3 coatings were insignificant. A similar trend was observed for the root mean square deviation (S_q).

The skewness (S_{sk}) and kurtosis (S_{ku}) were also measured, which are the two key parameters characterizing the asymmetry and the flatness of the surface distribution. The skewness parameter S_{sk} was close to zero, which was reflected in the symmetrical height distribution for the Ni/Al_2O_3-20 and Ni/Al_2O_3-80 + S coatings. The pure Ni showed negative skewness—0.867, indicating a surface with more deep and sharp valleys, while Ni/Al_2O_3-80 exhibited a positive value 0.879, describing a surface with peaks protruding from a mostly planar

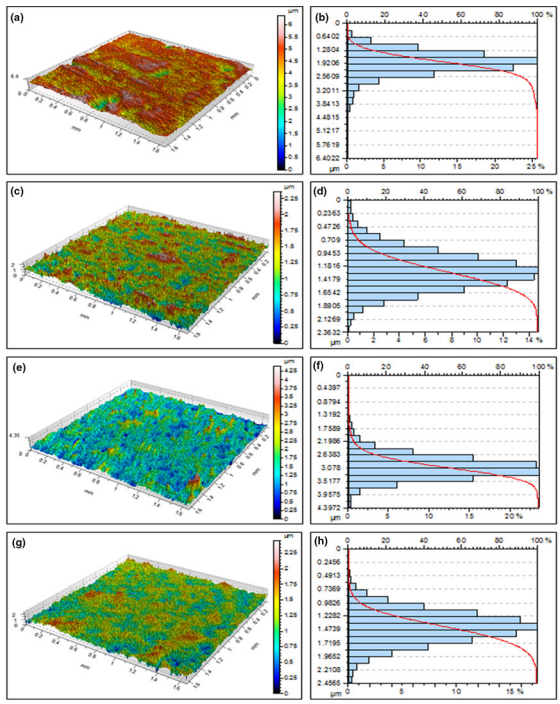

Fig. 5 Surface topography (a, c, e, g) and depth histogram with bearing curve (b, d, f, h) for coatings Ni (a, b) Ni/Al_2O_3-20 (c, d), Ni/Al_2O_3-80 (e, f) and Ni/Al_2O_3-80 + S (g, h)

surface. Additionally, higher values of kurtosis S_{ku} for both coatings were the result of larger grains in the profile of the surface. The other topography parameters, such as the maximum valley height S_v and the maximum height S_z, were significantly lower for the composite coatings compared to the pure Ni ones. A difference was only seen for the parameter of the maximum peak height S_p, which was the highest for Ni/Al_2O_3-80. It can be concluded that the deposited Ni/Al_2O_3 coatings revealed up to 45% lower roughness of their surfaces than the pure Ni coatings.

3.3 Residual Stresses of Coatings

The values of residual stresses are presented in Fig. 6. All the examined coatings revealed tensile residual stresses. Increasing the amount of incorporated Al_2O_3 nanopowder

Table 1 Surface topography parameters according to ISO 25178

Coating	Height parameters						
	S_a, µm	S_q, µm	S_{sk}	S_{ku}	S_p, µm	S_v, µm	S_z, µm
Ni	0.4147	0.5538	−0.8673	5.9688	1.8499	4.5523	6.4021
Ni/Al_2O_3-20	0.2582	0.3272	0.3024	3.3296	1.2502	1.1130	2.3632
Ni/Al_2O_3-80	0.3019	0.4030	0.8790	6.4893	3.0223	1.3749	4.3972
Ni/Al_2O_3 + S	0.2280	0.2892	−0.1038	3.2715	1.4196	1.0369	2.4565

S_a, arithmetic mean height; S_q, root mean squared height; S_{sk}, skewness; S_{ku}, kurtosis; S_p, maximum peak height; S_v, maximum valley depth; S_z, maximum height

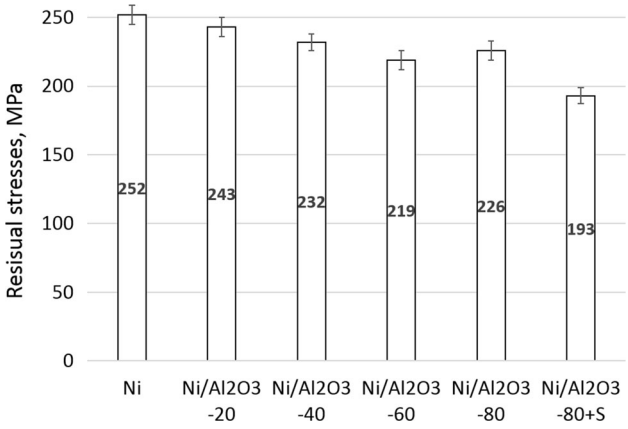

Fig. 6 Residual stresses determined in Ni and Ni/Al_2O_3 nanocomposite coatings obtained from the bath containing various amounts of Al_2O_3 and saccharin

resulted in a decrease in their values. The highest value of 252 MPa was revealed for the pure Ni coating and the lowest—193 MPa—for the Ni/Al_2O_3-80 + S sample obtained from the electrolyte with saccharin. The low residual stresses are connected with the considerable grain refinement of the Ni matrix. The grain size of nickel was smaller with a high Al_2O_3 nanoparticle content in the electrolyte, so that residual stresses could not accumulate as much as with larger grains (Ref 48). Taking into account the above considerations, it can be deduced that the saccharin additive is an effective residual stress reducer in the Ni/Al_2O_3 coatings. The character of the determined residual stresses agreed with those recorded by Erler et al. (Ref 48) for Ni/Al_2O_3 by means of in situ measurements of the strip contraction. They estimated lower values of stresses (less than 170 MPa), which was probably related to the content of sodium dodecyl sulfate in the electrolyte and a different method used to measure them. However, the estimated tensile stresses were in contradiction with the compressive stresses (−841.9 MPa) in Ni coatings produced with the use of pulse plating from a bath containing saccharin and sodium lauryl sulfonate, presented by El-Sherik et al. (Ref 49).

3.4 Mechanical Properties of Ni and Ni/Al_2O_3 Nanocomposite Coatings

The indentation microhardness (H) of the deposited Ni/Al_2O_3 nanocomposite coatings revealed the opposite tendency to that of the residual stresses (Fig. 7a). The improved microhardness due to the increased Al_2O_3 content in the deposited layer was highly correlated with the volume fraction of alumina. The microhardness in the coatings increased by about 30% with the increasing amount (up to 80 g/L) of Al_2O_3 in the bath. The Ni/Al_2O_3-80 composite coating containing 9.9 vol.% of incorporated Al_2O_3 had the microhardness of 4.4 GPa, whereas the pure Ni coating has 3.42 GPa. The obtained microhardness values were in the same range as the values for the Ni/Al_2O_3 nanocomposites containing nanoparticles reported by Corni et al. (Ref 50). With the increase in the ceramic phase content in the coatings, the grain size of the Ni matrix was decreased (Ref 17). Therefore, the increase in the microhardness values of the Ni/Al_2O_3 nanocomposites might be due to a smaller grain size of the Ni matrix favored by the nanosized Al_2O_3 particles. The increase in the microhardness values in the composite coatings was the result of a dispersion-strengthening effect by the Al_2O_3 nanoparticles, which impede the motion of dislocations in the metallic matrix, or the Orowan hardening mechanism (Ref 51). Nano-α-Al_2O_3 particles localized at the Ni grain boundaries inhibited the dislocation motion, restrained the growth of columnar grains of nickel and provoked the nucleation of new sites. Similar results were reported in other metal matrix nanocomposites, such as Ni-Al_2O_3 (Ref 11, 13, 28), Ni-CeO_2 (Ref 17) and Ni-SiC (Ref 18). However, the highest microhardness was revealed by the coatings obtained from the electrolyte with a saccharin additive. Taking into consideration the fact that, in this case, the amount of incorporated ceramic particles was smaller than in the composite coatings without saccharin (Fig. 4 and 7a), the higher hardness in this case is more strongly correlated with the refinement of the Ni matrix grains than with the embedding of Al_2O_3. The mechanism of saccharin acting as a grain refiner during the electrodeposition of Ni is due to: (i) blocking of the surface by the formation of complex deposits, which increases the frequency of nucleation and decreases the diffusion of the adsorbed Ni ions on the cathode, thus retarding the crystal growth (Ref 32-37), (ii) hydrogen evolution on the cathode, (iii) changing of the cathodic overpotential (Ref 32, 38). As presented in Ref 43 the effect of the saccharin on the Ni crystallite size refinement was much larger than that of Al_2O_3 nanoparticles. The Ni/Al_2O_3-80 + S coating possessed the crystallite size two times smaller than the Ni/Al_2O_3 coatings obtained from the bath without saccharin. The coatings with smaller grains had a larger grain boundary area and, consequently, higher microhardness. The presence of saccharin in the bath significantly enhanced the formation of growth-type nanotwins in the deposit. An increasing number of nanotwins in the matrix caused an increase in the coating microhardness

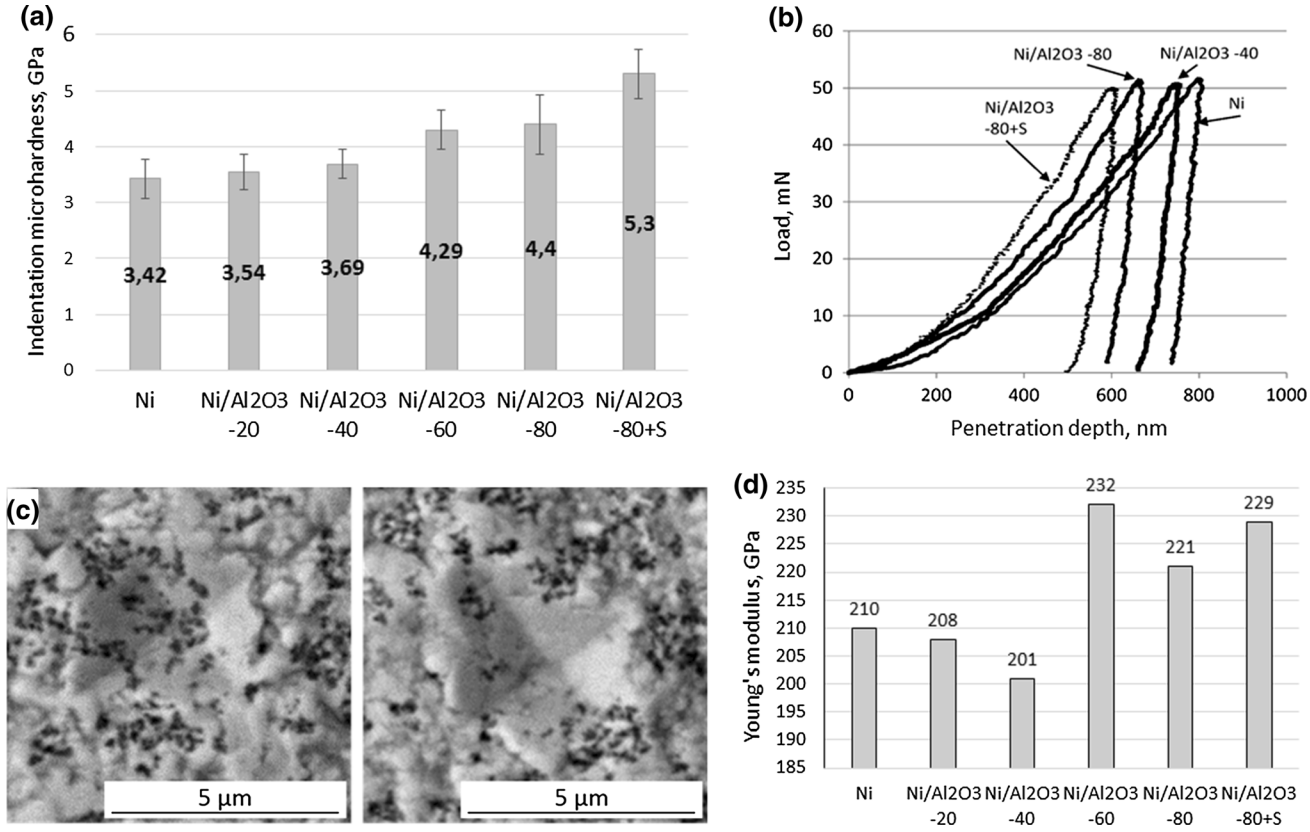

Fig. 7 Mechanical properties of the coatings: indentation microhardness (a), load-penetration depth behavior of Ni and Ni/Al_2O_3-40, Ni/Al_2O_3-80, Ni/Al_2O_3-80 + S (b), SEM BSE microstructures of indentation imprints on the surface of Ni/Al_2O_3-80 (c), Young's modulus of coatings (d)

Table 2 Results of microhardness and Young's modulus measured for Ni and Ni/Al_2O_3 coatings

Coating	Indentation microhardness *H*, GPa	Young's modulus *E*, GPa	*H*/*E*
Ni	3.42 ± 0.35	210 ± 8	0.0163
Ni/Al_2O_3-20	3.54 ± 0.32	208 ± 4	0.0170
Ni/Al_2O_3-40	3.69 ± 0.27	201 ± 10	0.0184
Ni/Al_2O_3-60	4.29 ± 0.35	232 ± 12	0.0185
Ni/Al_2O_3-80	4.40 ± 0.53	221 ± 18	0.0199
Ni/Al_2O_3 + S	5.30 ± 0.44	229 ± 14	0.0231

because the nanotwin boundaries blocked the motion of dislocations in the matrix to obtain higher mechanical strength.

Figure 7(b) presents an exemplary indentation load versus penetration depth hysteresis for Ni and three Ni/Al_2O_3 nanocomposite coatings. The lowest penetration depth at 50 mN load was obtained for the Ni/Al_2O_3-80 + S coatings obtained from the electrolyte with the saccharin additive and the highest penetration depth for the pure Ni deposit, which correlates inversely with the results of microhardness presented in Fig. 7(a). The SEM images (Fig. 7c) of the indents after the Vickers indentation showed an elasto-plastic character of the deformation. No circumferential or corner cracks were found for the nanocomposite coatings. Additionally, the indentation imprint observed in the area containing more of the ceramic phase was approximately the same as that in the area with fewer particles, which indicates that the amount of the ceramic phase could be higher under the indent. This testifies the coating's homogeneity, which was confirmed by only a 10% scatter of the indentation results.

The results of Young's modulus measured for the coatings produced from the bath containing various amounts of a ceramic phase and saccharin are presented in Fig. 7(d). Young's modulus remained on the level of 210-232 GPa. The highest values were revealed by the coatings Ni/Al_2O_3-60 (232 GPa) and Ni/Al_2O_3-80 + S (229 GPa). Interestingly, these values of E corresponded to the lowest values of residual stresses in these coatings, 219 and 193 MPa, respectively. Moreover, the ratio between the microhardness (*H*) and the elastic modulus (*E*) was calculated, because, as presented by Leyland et al. (Ref 52), it might be a suitable parameter for the foreseeing of the wear behavior of a coating. It was so-called elastic strain to failure (*H*/*E*), and it is considered as a reliable indicator of a good wear resistance in a coating. According to Ref 52, the most durable coatings can be obtained if *H*/*E* has a high value, i.e., sufficiently high hardness (to resist plastic deformation), but with a low elastic modulus (similar to, or slightly below that of the substrate material). The values of *H*/*E* calculated for the Ni, Ni/Al_2O_3-20, Ni/Al_2O_3-40, Ni/Al_2O_3-60 Ni/Al_2O_3-80 and Ni/

Al_2O_3-80 + S coatings are presented in Table 2. They show that the best wear resistance should be exhibited by the Ni/Al_2O_3-80 + S coating. In the case of the other Ni/Al_2O_3 nanocomposite coatings, the wear resistance should increase with the increasing amount of the ceramic particles incorporated into the coating.

3.5 Tribological Properties of Ni and Ni/Al_2O_3 Coatings

The wear behavior of the Ni and Ni/Al_2O_3-20, Ni/Al_2O_3-40, Ni/Al_2O_3-60, Ni/Al_2O_3-80, Ni/Al_2O_3-80 + S coatings was examined under dry sliding conditions. The measurements of the friction track profiles of the samples showed the presence of high volumes of uplifted material located at both sides of the groove. As the size of these uplifted materials was 15-20% of the grooves, they were taken into account in the calculation of the wear index. The volume of the waste material was the volume of the grooves reduced by the uplifted volume. The wear resistances of the Ni/Al_2O_3 nanocomposite coatings were strongly related to the Al_2O_3 nanoparticles content in the Ni matrix. Figure 8 shows the relationship between the particles concentration in the electrolyte and the wear index. The results indicated that the wear resistance increased with the Al_2O_3 particles content in the electrolyte and later the volume fraction of nanoalumina in the deposited layer. It is evident from Fig. 8-10 that the Ni/Al_2O_3 nanocomposite coatings exhibited a better wear resistance than the pure Ni coating in a sliding contact with the alumina ball. The Ni/Al_2O_3-80 coating exhibited a three times lower wear than the Ni coating and the specific wear rate reached the value of 0.9×10^{-6} and 2.9×10^{-6} mm^3/Nm, respectively. This wear index was in the same range as the value reported by Aruna et al. (Ref 12) (9.419 10^{-7} for a Ni/Al_2O_3 coating with α-Al_2O_3 nanoparticles). This can be attributed to the hard nature of the reinforcements and the dispersion-strengthening effect with the incorporation of the ceramic nanoparticles. As shown in Fig. 3, the coatings structure contained numerous nanotwins. There were the growth-type (111) nanotwins observed along the [011] zone axis and their size decreased with the increasing amount of built Al_2O_3 nanoparticles and decreasing size of Ni grains (Ref 43). The higher nucleation, due to the nanoparticle incorporation, disturbed the growth of the nickel matrix and resulted in its smaller grain size. The nanocrystalline matrix besides nanotwins revealed other structure defects, such as stacking faults and dislocations. The most number of these defects was observed in the structure of the Ni/Al_2O_3-80 + S coatings. These coatings with the smallest the grain size revealed the smallest twin lamellae, and the highest mechanical and tribological properties. This is related to the fact that dislocation motion in the matrix is blocked by the nanotwin boundaries, and therefore, they required the higher external stress to cross the twin boundary. Such morphology was beneficial for the improvement in the wear resistance, since it could increase the load-carrying capacity of the coatings. In this

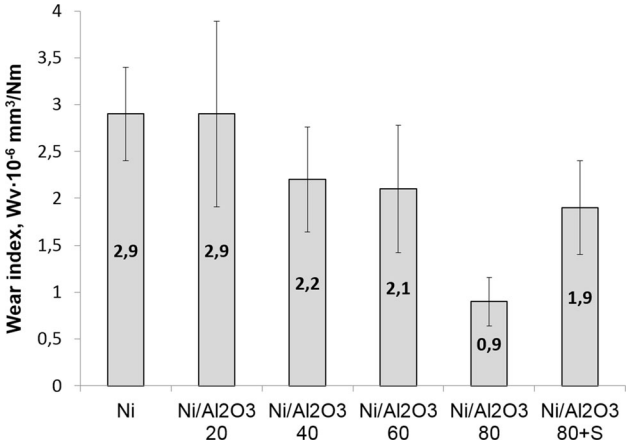

Fig. 8 Wear index determined for pure Ni and Ni/Al_2O_3 nanocomposite coatings produced from the electrolyte containing various amounts Al_2O_3 nanoparticles and saccharin additive

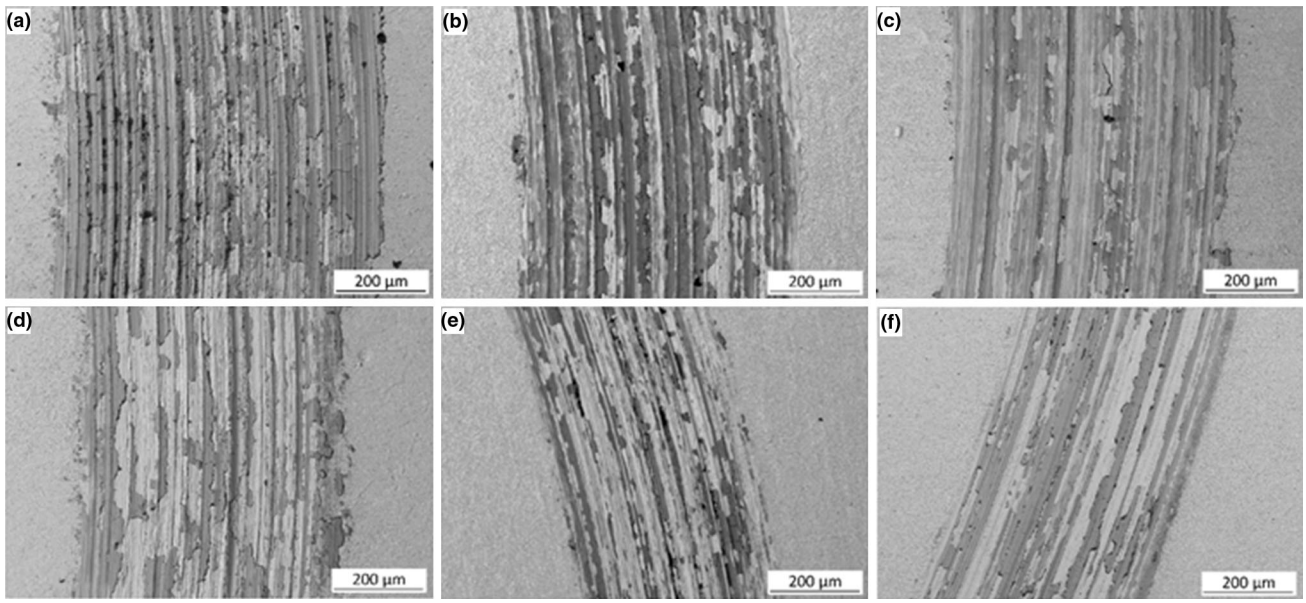

Fig. 9 SEM BSE microstructures of wear tracks after wear tests of coatings: Ni (a), Ni/Al_2O_3-20 (b), Ni/Al_2O_3-40 (c), Ni/Al_2O_3-60 (d), Ni/Al_2O_3-80 (e), Ni/Al_2O_3-80 + S (f)

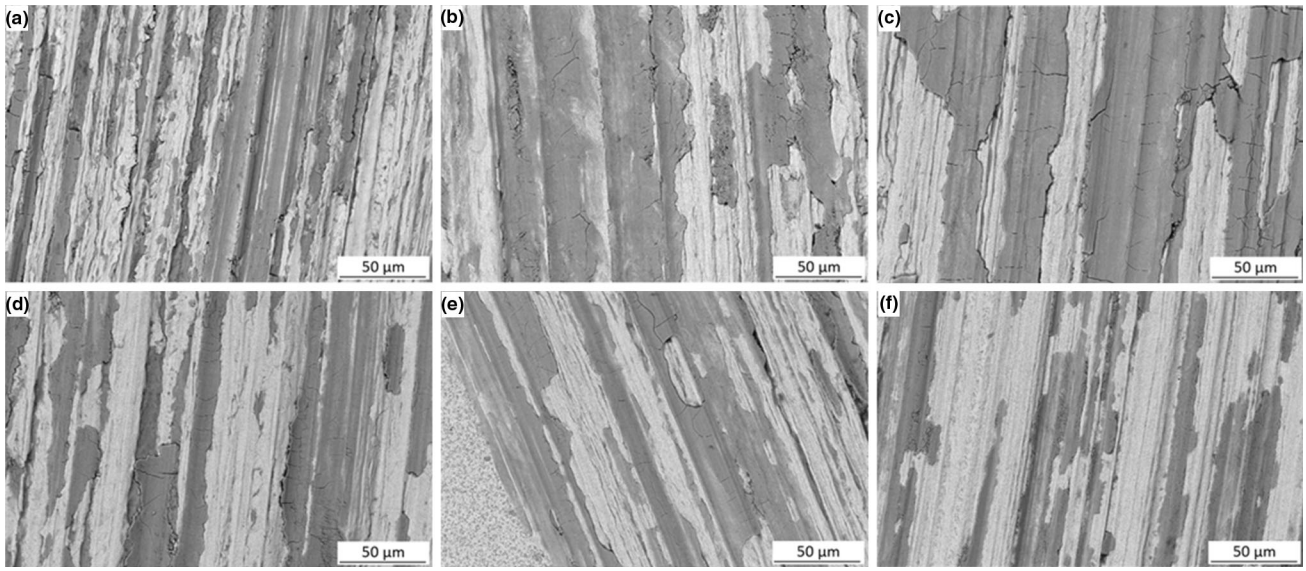

Fig. 10 High magnification SEM BSE microstructures of wear tracks after wear tests of the coatings: Ni (a), Ni/Al_2O_3-20 (b), Ni/Al_2O_3-40 (c), Ni/Al_2O_3-60 (d), Ni/Al_2O_3-80 (e), Ni/Al_2O_3-80 + S (f)

case, the matrix carried the load and the fine particles impeded the motion of dislocations (Ref 53). With the grain refinement of the Ni matrix, the load-carrying capacity and the resistance to plastic deformation increased (Ref 18). It was especially visible in the case of the Ni/Al_2O_3-80 + S coating, where it was impossible to calculate the wear index after 20,000 cycles. A destruction of this coating was constituted by a plurality of scratches which were observed in the area of the friction track. However, an apparent deep wiping was not visible. That is why additional tests in an extended time (80,000 cycles) of the sample's collaboration with the ball surface were performed. The wear of this coating was abrasive. The volume of the uplifted material on both sides of the grooves comprised 7% of the total volume of the furrow, so it was negligible and did not take a significant part in the fissuring. The coating revealed the highest wear resistance of all the examined Ni/Al_2O_3 coatings.

The incorporated nanoparticles reduced the direct contact between the metal matrix and the Al_2O_3 ball during the tribological test, which reduced the adhesive wear between the metal and the ball. The wear mechanism of pure nickel and the composite coatings was analyzed by SEM observations of the wear tracks, as shown in Fig. 9 and 10. From the low magnification SEM micrographs (Fig. 9), it can be seen that the lowest wear appeared in the coating produced from the bath containing 80 g/L Al_2O_3 and 1 g/L saccharin. The Ni/Al_2O_3 coatings obtained from the bath containing more than 40 g/L Al_2O_3 particles exhibited a better wear resistance than the pure Ni coating when sliding against the alumina ball. Compared with the pure Ni coating, the worn surface of the Ni/Al_2O_3 composite coatings decreased with the increasing amount of the ceramic particles. Wear track of pure Ni coating exhibited dominant adhesive wear mechanism, whereas Ni/Al_2O_3 composites showed a preferably abrasive type of wear, whose predominance increased with the increasing alumina content. Some rows of grooves, smearing and plastic deformation were seen in wear tracks at higher magnification SEM images, as shown in Fig. 10. The plastic deformation occurred by smearing of the wear debris on the alumina ball was also observed. The surfaces of Ni/Al_2O_3 showed plastic deformation with microcracks of worn layers transferred between the counter body ball and the composite interfaces. The higher amount of Al_2O_3 nanoparticles in the coatings reduced plastic deformation zones and changed the wear type to abrasion. Some delamination was the result of debris smearing on the composite surfaces, and fatigue crack growth mechanisms subsequently caused material removal from the composite surfaces. An addition of the saccharin to the electrolyte produced less amount of wear debris smeared on the surface. The higher vol.% of the Al_2O_3 nanoparticles incorporated into the coating enhanced the coating's degree of wear resistance, which may be attributed to the higher microhardness corresponding to the higher load bearing capability and lower ductility (Ref 54). The better wear coating resistance indicated the high strength of the particles to the metal matrix bonds.

It was shown that, after a short running-in stage at the beginning of the test, the friction coefficient (COF) of nanocomposites entered a steady-state period. However, for Ni/Al_2O_3-80 + S, similarly as for the Ni coating, it exhibited a change during 18,000 cycles, maintaining an upward trend by keeping a stable value during the test of 0.31 and 0.45, respectively. The same character of the curves suggested the friction coefficient in this composite depending to a large extent on the matrix characteristics. The other Ni/Al_2O_3 nanocomposites showed a much more stable friction coefficient with a similar value (0.31-0.34), as shown in Fig. 11, and its value did not change significantly with the increasing ceramic particle content in the electrolyte. Figure 11 shows that the Ni/Al_2O_3 nanocomposites exhibited a lower friction coefficient (more than 30%) than the Ni deposit under identical wear test conditions. The coatings Ni/Al_2O_3-20 and Ni/Al_2O_3-40 showed practically the same values 0.31, the coatings Ni/Al_2O_3-80—0.34, and the smallest value was achieved for Ni/Al_2O_3-60. The lower friction coefficient can be explained in terms of good interfacial bonding between Ni and the ceramic particles. The fine surface morphology of the nanocomposite coating probably increased the load-carrying area and reduced the stress between the friction couples. The lower friction coefficient of

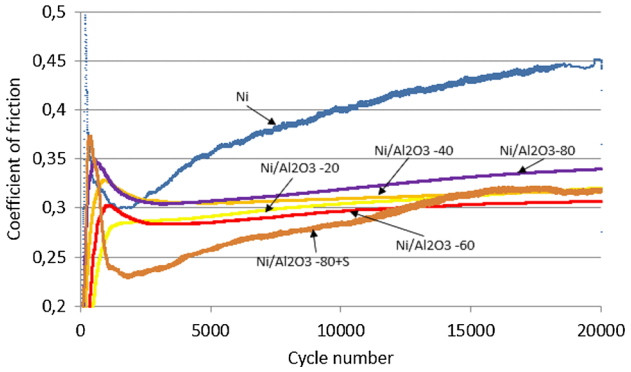

Fig. 11 Variation of the friction coefficient of nickel and Ni/Al_2O_3 nanocomposite coatings with sliding cycles

the composite coating could be explained by the "microball bearing" effect of the nanoparticles during sliding (Ref 28). The presented values of COF are much lower than those obtained by Aruna et al. (0.819) and Saha et al. (0.5) (Ref 12, 31). Gul et al. (Ref 11) have shown changes of the coefficient of friction depending on the kind and values of the current density as well as the sliding speed determined for the coatings obtained from the bath containing HPB surfactant. They demonstrated that the coefficient of friction decreased with the increasing sliding speed and it achieved the value below 0.2 for the sliding speed of 150 mm/s.

3.6 Correlation Between Surface Topography and Friction Coefficient as Well as Wear Resistance

The friction coefficient was found to depend on the surface roughness, and it was higher for rougher surfaces. The performed examinations showed that the pure Ni coatings revealed the highest friction coefficient (Fig. 11). In general, we can ascertain that this coating exhibited the values of all the surface topography parameters being significantly higher than those of the composite Ni/Al_2O_3 coatings. The Ni coating revealed a deviation from the Gaussian distribution with the surfaces of negative asymmetry ($S_{sk} = -0.867$) and great sharpness of the profile ($S_{ku} = 5.9688$). Of all the Ni/Al_2O_3 composite coatings, that obtained from the bath containing 80 g/L α-Al_2O_3 showed the highest COF, which was, however, significantly lower than that of the Ni coating. It can also be noticed that the friction tends to be lower for the coatings Ni/Al_2O_3-20, Ni/Al_2O_3-40, Ni/Al_2O_3-80 + S—its value was almost the same after 20,000 cycles (Fig. 11). This agreed with the surface topography parameters determined for the Ni/Al_2O_3-20, Ni/Al_2O_3-80 + S coatings, which were very similar (Table 1). Moreover, the skewness parameter S_{sk} was close to zero and the kurtosis S_{ku} was close to 3, which proves the Gaussian-type distribution ($S_{sk} = 0$, $S_{ku} = 3$). The Ni/Al_2O_3-80 coating revealed significantly higher values of each measured parameter, which was reflected in a slightly higher friction coefficient (Fig. 11). Interestingly, although Ni/Al_2O_3-80 disclosed a similar kurtosis as the Ni coating, the skewness parameter ($S_{sk} = 0.879$) was positive, contrary to Ni. The obtained results stayed in agreement with (Ref 39), who showed that a positive skewness reduced the coefficient of friction, while in the case of a negative skewness, the friction is more intense than the Gaussian distribution.

Regarding the wear resistance of the coatings, it did not show a distinct dependence on the surface topography, as is the case of the friction coefficient. Instead, the wear resistance of the coatings corresponded very well with the predictions resulting from the determined values of H/E. The best wear resistance was revealed by the Ni/Al_2O_3-80 + S coating, which was related to a significant grain refinement of the Ni matrix.

4. Conclusions

This paper presents a characterization of the surface topography, as well as the mechanical and tribological properties of thin nanocomposite Ni/Al_2O_3 coatings electrodeposited from the Watt's bath containing various amounts (20, 40, 60, 80 g/L) of Al_2O_3 nanoparticles. The obtained results are shown below.

1. The co-deposition of α-Al_2O_3 particles into the nickel matrix provided a refinement of the nickel grain sizes and a significant improvement in the coating properties, such as microhardness, wear resistance and friction coefficient, compared with the pure nickel coatings.
2. The Ni/Al_2O_3 nanocomposite coatings showed an evident relationship between their composition and microhardness, which increased (30%) with the increase in the amounts of incorporated particles (up to 9.9 vol.%). This was because the composite coating was strengthened by the fine crystal and the hard particle dispersion intensification. The coating's hardening corresponded to the rise in the wear resistance.
3. The incorporation of Al_2O_3 into the Ni matrix improved the wear resistance of the Ni deposits. The wear index decreased with the rise in the amount of alumina nanoparticles. The Ni/Al_2O_3-80 coatings deposited from the solution containing 80 g/L of Al_2O_3 exhibited a three times lower wear index than the pure Ni coatings.
4. The friction coefficient was found to depend on the surface roughness, and it was lower for smoother surfaces of the coatings. The wear resistance of the coatings did not show a distinct dependence on the surface topography. It affected only the initial process of wear.
5. All the coatings revealed tensile residual stresses, which were insignificantly (20%) reduced as the amount of incorporated Al_2O_3 nanoparticles increased.
6. The addition of 1 g/L of saccharin into the electrolyte did not enhance the incorporation of ceramic particles into the coating. However, it had a positive impact on the microstructure refinement of the matrix, the microhardness increase and the residual stress reduction in the coatings.
7. Compared to the electrodeposited pure nickel, the Ni/Al_2O_3 composite with nanoparticles exhibited a higher microhardness and a better wear resistance. The best mechanical and tribological properties were revealed by the Ni/Al_2O_3-80 + S coating.
8. The studies have shown that the friction coefficient and the wear resistance of the Ni/Al_2O_3 coatings can be predicted in advance on the basis of the surface roughness measurements and the elastic strain to failure calculations (H/E). The Ni/Al_2O_3 nanocomposite coatings were characterized by a low wear index and friction coefficient, which is very promising in the perspective of their use as a replacement for hard chromium coatings.

Acknowledgments

This work is supported by National Science Centre of Poland (Project No. 2011/01/D/ST8/05318).

References

1. ASM Handbook, *5A: Thermal Spray Technology*, ASM International, 2013
2. A. Góral, J. Deda, E. Bełtowska-Lehman, and B. Major, Analysis of Strengths, Weaknesses, Opportunities and Threats (SWOT) and Prerequisite Tree (PT) of Selected Technologies for Coating and Layer Production, *Arch. Metall. Mater.*, 2008, **53**, p 979–984
3. W. Żórawski and S. Kozerski, Scuffing Resistance of Plasma and HVOF Sprayed WC12Co, $Cr_3C_2$25 (Ni20Cr) Coatings, *Surf. Coat. Technol.*, 2008, **202**, p 4453–4457
4. W. Żórawski and S. Skrzypek, Tribological Properties of Plasma and HVOF Sprayed NiCrBSi-Fe_2O_3 Composite Coatings, *Surf. Coat. Technol.*, 2013, **220**, p 276–281
5. N.S. Qu, D. Zhu, K.C. Chan, and W.N. Lei, Pulse Electrodeposition of Nanocrystalline Nickel Using Ultra Narrow Pulse Width and High Peak Current Density, *Surf. Coat. Technol.*, 2003, **168**, p 123–128
6. I. Napłoszek-Bilnik, A. Budniok, B. Łosiewicz, L. Pająk, and E. Łagiewka, Electrodeposition of Composite Ni-Based Coatings with the Addition of Ti or/and Al Particles, *Thin Solid Films*, 2005, **474**, p 146–153
7. A. Hovestad and L.J.J. Jansen, Electrochemical Codeposition of Inert Particles in a Metallic Matrix, *J. Appl. Electrochem.*, 1995, **25**, p 519–527
8. S.W. Banovic, K. Barmak, and A.R. Marder, Characterization of Single and Discretely-Stepped Electro-Composite Coatings of Nickel-Alumina, *J. Mater. Sci.*, 1999, **34**, p 3203–3211
9. L. Chen, L. Wang, Z. Zeng, and J. Zhang, Effect of Surfactant on the Electrodeposition and Wear Resistance of Ni-Al_2O_3 Composite Coatings, *Mater. Sci. Eng. A Struct.*, 2006, **434**, p 319–325
10. H. Gul, F. Kilic, S. Aslan, A. Alp, and H. Akbulut, Characteristics of Electro-Co-deposited Ni-Al_2O_3 Nano-Particle Reinforced Metal Matrix Composite (MMC) coatings, *Wear*, 2009, **267**, p 976–990
11. H. Gül, M. Uysal, H. Akbulut, and A. Alp, Effect of PC Electrodeposition on the Structure and Tribological Behaviour of Ni-Al_2O_3 Nanocomposite Coatings, *Surf. Coat. Technol.*, 2014, **258**, p 1202–1211
12. S.T. Aruna, V.E. Selvi, V.K.W. Grips, and K.S. Rajam, Corrosion- and Wear-Resistant Properties of Ni-Al_2O_3 Composite Coatings Containing Various Forms of Alumina, *J. Appl. Electrochem.*, 2011, **41**, p 461–468
13. A. Góral, M. Nowak, K. Berent, and B. Kania, Influence of Current Density on Microstructure and Properties of Electrodeposited Nickel-Alumina Composite Coatings, *J. Alloys Compd.*, 2014, **615**, p S406–S410
14. Y.-H. You, C.-D. Gu, X.-L. Wang, and J.-P. Tu, Electrochemical Preparation and Characterization of Ni-PTFE Composite Coatings from a Non-aqueous Solution Without Additives, *Int. J. Electrochem. Sci.*, 2012, **7**, p 12440–12455
15. Z. Shafiee, M.E. Bahrololoom, and B. Hashemi, Electrodeposition of Nanocrystalline Ni/Ni-Al_2O_3 Nanocomposite Modulated Multilayer Coatings, *Mater. Des.*, 2016, **108**, p 19–26
16. M.H. Allahyarzadeh, M. Aliofkhazraei, A.R. Sabour Rouhaghdam, and V. Torabinejad, Electrodeposition of Ni-W-Al_2O_3 Nanocomposite Coating with Functionally Graded Microstructure, *J. Alloys Compd.*, 2016, **666**, p 217–226
17. N.S. Qu, D. Zhu, and K.C. Chan, Fabrication of Ni-CeO_2 Nanocomposite by Electrodeposition, *Scr. Mater.*, 2006, **54**, p 1421–1425
18. Y. Zhou, H. Zhang, and B. Qian, Friction and Wear Properties of the Co-deposited Ni-SiC Nanocomposite Coatings, *Appl. Surf. Sci.*, 2007, **253**, p 8335–8339
19. X.J. Sun and J.G. Li, Friction and Wear Properties of Electrodeposited Nickel-Titania Nanocomposite Coatings, *Tribol. Lett.*, 2007, **28**, p 223–228
20. K.H. Hou and Y.C. Chen, Preparation and Wear Resistance of Pulse Electrodeposited Ni-W/Al_2O_3 Composite Coatings, *Appl. Surf. Sci.*, 2011, **257**, p 6340–6346
21. Directive RoHS (Restriction of Hazardous Substances) 2002/95/EU
22. Directive RoHS 2011/65/EU (RoHS 2)
23. Directive 2000/53/EC—the ELV Directive
24. S. Steinhauser and B. Wielage, Composite Coatings: Manufacture, Properties, and Applications, *Surf. Eng.*, 1997, **13**, p 289–294
25. S.-L. Kuo, Y.-C. Chen, M.-D. Ger, and W.-H. Whu, Nano-Particles Dispersion Effect on Ni/Al_2O_3 Composite Coatings, *Mater. Chem. Phys.*, 2004, **86**, p 5–10
26. B. Szczygieł and M. Kołodziej, Composite Ni/Al_2O_3 Coatings and Their Corrosion Resistance, *Electrochim. Acta*, 2005, **50**, p 4188–4195
27. *Technical Tidbits a publication by Brush Wellman Engineered Materials*, 2002, vol 4, p 4
28. L. Du, B. Xu, S. Dong, H. Yang, and Y. Wu, Preparation, Microstructure and Tribological Properties of Nano-Al_2O_3-Ni Brush Plated Composite Coatings, *Surf. Coat. Technol.*, 2005, **192**, p 311–316
29. J. Steinbach and H. Ferkel, Nanostructured Ni-Al_2O_3 Films Prepared by DC and Pulsed DC Electroplating, *Scr. Mater.*, 2001, **44**, p 1813–1816
30. D. Thiemig, A. Bund, and J.B. Talbot, Influence of Hydrodynamics and Pulse Plating Parameters on the Electrodeposition of Nickel-Alumina Nanocomposite Films, *Electrochim. Acta*, 2009, **54**, p 2491–2498
31. R.K. Saha and T.I. Khan, Effect of Applied Current on Electrodeposited Ni-Al_2O_3 Composite Coatings, *Surf. Coat. Technol.*, 2010, **205**, p 890–895
32. Y. Nakamura, N. Kaneko, M. Watanabe, and H. Nezu, Effects of Saccharin and Aliphatic Alcohols on the Electrocrystallization of Nickel, *J. Appl. Electrochem.*, 1994, **24**, p 227–232
33. Y. Xuetao, W. Yu, S. Dongbai, and Y. Hongying, Influence of Pulse Parameters on the Microstructure and Microhardness of Nickel Electrodeposits, *Surf. Coat. Technol.*, 2008, **202**, p 1895–1903
34. A.M. El-Sherik and U. Erb, Synthesis of Bulk Nanocrystalline Nickel by Pulsed Electrodeposition, *J. Mater. Sci.*, 1995, **30**, p 5743–5749
35. R.T.C. Choo, J. Toguri, A.M. El-Sherik, and U. Erb, Mass Transfer and Electrocrystallization Analyses of Nanocrystalline Nickel Production by Pulse Plating, *J. Appl. Electrochem.*, 1995, **25**, p 384–403
36. D. Mockute and G. Bernotiene, The Interaction of Additives with the Cathode in a Mixture of Saccharin, 2-Butyne-1,4-diol and Phthalimide During Nickel Electrodeposition in a Watts-Type Electrolyte, *Surf. Coat. Technol.*, 2000, **135**, p 42–47
37. A.M. Rashidi and A. Amadeh, The Effect of Saccharin Addition and Bath Temperature on the Grain Size of Nanocrystalline Nickel Coatings, *Surf. Coat. Technol.*, 2009, **204**, p 353–358
38. B. Szeptycka, Effects of Organic Compounds on the Electrocrystallization of Nickel, *Russ. J. Electrochem.*, 2001, **37**, p 684–689
39. N. Tayebi and A.A. Polycarpou, Modeling the Effect of Skewness and Kurtosis on the Static Coefficient of Rough Surfaces, *Tribol. Int.*, 2004, **37**, p 491–505
40. F. Svahn, Å. Kassman-Rudolphi, and E. Wallén, The Influence of Surface Roughness on Friction and Wear of Machine Element Coatings, *Wear*, 2003, **254**, p 1092–1098
41. R.A. Al-Samarai, Haftirman, K.R. Ahmad, and Y. Al-Douri, The Influence of Roughness on the Wear and Friction Coefficient under Dry and Lubricated Sliding, *Int. J. Sci. Eng. Res.*, 2012, **3**, p 1–6
42. A. Góral, M. Nowak, and J. Wojewoda-Budka, Influence of Surfactants on Microstructure and Corrosion Resistance of Ni/Al_2O_3 Coatings, *Mater. Eng.*, 2013, **3**, p 165–168
43. A. Góral, Nanoscale Structural Defects in Electrodeposited Ni/Al_2O_3 Composite Coatings, *Surf. Coat. Technol.*, 2017, **319**, p 23–32
44. M. Kot and P. Lacki, Contact Mechanics of Coating-Substrate Systems: I—Methods of Analysis and FEM Modeling of Nanoindentation Tests, *J. Balk. Tribol. Assoc.*, 2012, **18**, p 598–614

45. ISO 14577-1:2002, Metallic Materials—Instrumented Indentation Test for Hardness and Material Parameters—Part 1: Test Method
46. ISO 20808:2004. Fine Ceramics (Advanced Ceramics, Advanced Technical Ceramics)—Determination of Friction and Wear Characteristics of Monolithic Ceramics by Ball-on-Disc Method
47. S. Adamczak, D. Janecki, and K. Stępień, Cylindricity Measurement by the V-Block Method—Theoretical and Practical Problems, *Measurement*, 2011, **44**(1), p 164–173
48. F. Erler, C. Jacob, H. Romanus, L. Spiess, B. Wielage, T. Lampke, and S. Steinhauser, Interface Behaviour in Nickel Composite Coatings with Nano-Particles of Oxidic Ceramic, *Electrochim. Acta*, 2003, **48**, p 3063–3070
49. A.M. El-Sherik, J. Shirokoff, and U. Erb, Stress Measurements in Nanocrystalline Ni Deposits, *J. Alloys Compd.*, 2005, **389**, p 140–143
50. I. Corni, L. Chen, L. Wang, Z. Zeng, and J. Zhang, Effect of Surfactant on the Electrodeposition and Wear Resistance of Ni-Al_2O_3 Composite Coatings, *Mater. Sci. Eng. A Struct. A*, 2006, **434**, p 319–325
51. V.P. Greco, Electrocomposites and Their Benefits, *Plat. Surf. Finish.*, 1989, **7**, p 62–67
52. A. Leyland and A. Matthews, On the Significance of the H/E Ratio in Wear Control: A Nanocomposite Coating Approach to Optimised Tribological Behaviour, *Wear*, 2000, **246**, p 1–11
53. B. Muller and H. Ferkel, Al_2O_3-Nanoparticle Distribution in Plated Nickel Composite Films, *Nanostruct. Mater.*, 1998, **10**, p 1285–1288
54. N.K. Shrestha, K. Sakurada, M. Masuko, and T. Saji, Composite Coatings if Nickel and Ceramic Particles Prepared in Two Steps, *Surf. Coat. Technol.*, 2001, **140**, p 175–181